Journal of Magnetic Resonance **138,** 199–209 (1999)
Article ID jmre.1999.1737, available online at http://www.idealibrary.com on IDEAL®

Linewidth Analysis of Spin Labels in Liquids

I. Theory and Data Analysis

B. H. Robinson, C. Mailer, and A. W. Reese

Department of Chemistry, University of Washington, Seattle, Washington 98195

Received July 28, 1998; revised February 12, 1999

We present a method of simulating the EPR spectra of spin labels in liquids using direct convolution of hyperfine splitting with Lorentzian linewidths. The aim is to simulate the experimental lineshape by considering all spectrometer characteristics as well as inhomogeneous and homogenous linewidth effects. A major advance in this method is the correction for the broadening produced by Zeeman modulation commonly used to obtain EPR signals; this allows experimenters much more freedom to optimize their experimental conditions for the best signal-to-noise ratio. Microwave power broadening (saturation) effects on the EPR lines are significant even at very low observer levels. Successful simulation requires that all contributions from unresolved hyperfine splittings be explicitly included. Inhomogeneous broadening is dealt with by including all spins that interact with the electron (as a set of superhyperfine interactions); there is no "effective Gaussian" to substitute for the correct superhyperfine interactions. The effects of spin exchange on the linewidth and lineshape can be observed and must be taken into account in order to extract the fundamental linewidths.

Key Words: **linewidth; lineshape; EPR spin labels; simulation; exchange.**

INTRODUCTION

The aim of this paper (Paper I) is to provide the background and theoretical framework for us to answer the simple question: Can all broadening seen in electron paramagnetic resonance (EPR) spectra of the lines from nitroxide spin labels be quantitated? We consider nitroxide spin labels in liquids undergoing rapid rotational motion (characterized by correlation times smaller than a few nanoseconds). There are many proposals in the literature (*1*) that suggest how to extract the molecular rotational correlation times from continuous wave (CW) EPR spectra. One method is to measure the homogeneous linewidths (identical to those observed by electron spin echo (pulsed) experiments) and determine the motional properties of the spin label from them.

However, extracting these linewidths directly from the CW EPR lineshape is problematic because the CW EPR line contains broadening effects (artifacts) due to the spectrometer detection principles: the effect of dispersion mixed in with the absorption signal, the effect of the finite level of the microwave field, and the effects of the Zeeman modulation. The spectra have different intrinsic homogeneous linewidths for each of the lines due to the interaction of the electron with the nitrogen nucleus. Additional inhomogeneous broadening due to the superhyperfine interactions of the electron with the protons (or deuterons) and the (^{13}C) carbons of the label also occurs. To our knowledge no one has examined these sources of broadening with the aim of quantitatively accounting for all sources of line broadening simultaneously in spin labeled EPR experiments. We have done so in this work and will use the resulting data to study motion of spin labels in solution in the accompanying paper (Paper II). In this paper (I) the linewidth analysis techniques used are described and experimental results presented. A brief description of this work has been given elsewhere (*2*). We now present the sources of broadening and how they are all, simultaneously, taken into account.

INSTRUMENTAL BROADENING MECHANISMS

Absorption/dispersion phase rotation. In normal CW EPR spectroscopy only the absorption component of the resonance signal is observed with the dispersion component being suppressed by suitable phasing of the microwave bridge. In principle the microwave phase in the reference arm of modern EPR bridges can be set to give a pure, symmetric absorption-shaped signal. In practice for a standard TE_{102} cavity the phasing is within 1–2° of that for pure absorption, while in a loop gap resonator (*3*) the error can be as much as 20°. Some dispersion component is therefore always present in the signals and must be taken into account. This is done by combining the simulated pure absorption EPR signal (A) with the dispersion signal (D) for a total signal of $S = A\cos(\theta) + D\sin(\theta)$.

Observer RF field amplitude. Linewidths can become very narrow—50–70 mG at a rotational correlation time of 30 ps (typical of a spin label in deoxygenated water). Does the microwave observer RF field amplitude, h_1 (typically 30–40 mG) produce extra broadening due to line saturation? The

1090-7807/99 $30.00

equation for line broadening (assuming no Zeeman modulation effects on relaxation (*4*)) is given by

$$R_{2eobs}^2 = R_{2e}^2(1 + h_1^2/R_{1e}R_{2e}), \quad [1]$$

where R_{2eobs} is the observed homogeneous linewidth, R_{2e} is the intrinsic unbroadened homogeneous linewidth, and R_{1e} is the spin–lattice relaxation rate, all expressed in the same units. This quadratic in R_{2eobs} can be rearranged to give the corrected linewidth R_{2e} in terms of experimental observables:

$$R_{2e} = -h_1^2/2R_{1e} + \sqrt{(h_1^2/2R_{1e})^2 + R_{2eobs}^2}. \quad [2]$$

For typical values of R_{1e} and h_1 the correction can be as much as 25% of R_{2eobs}, so saturation effects are important.

Zeeman modulation frequency, modulation amplitude, and phase. Modulation of the Zeeman field at frequencies between 10 and 100 kHz is universally employed in CW EPR spectroscopy to increase the signal-to-noise ratio (SNR) (*5*). This action, however, produces significant line broadening if the modulation amplitude or frequency (expressed in gauss) is a significant fraction of the intrinsic linewidth. The usual procedure is to reduce the modulation amplitude to less than the narrowest observed linewidth R_{2eobs}; in fact one should really reduce the amplitude to less than the narrowest intrinsic linewidth R_{2e}. Either way one pays a big price in the SNR. Ideally one would like to be able to increase the Zeeman modulation amplitude to give maximum signals from the lines in the spectrum (the Zeeman frequency also produces broadening but this is usually less important). The effects of Zeeman modulation and frequency are not routinely included in EPR simulations; the simple corrections shown below mean that they can be.

We have developed an exact method of lineshape simulation that gives the true linewidths even when the lines are overmodulated. The theory described below is developed from that for CW saturation-transfer EPR—a technique to obtain motional information using the quadrature signal at the second harmonic of the Zeeman modulation—which requires that modulation effects be explicitly included (*6*, *7*). We can correct for any imperfections in settings of quadrature phasing and take into account the finite broadening effects of modulation amplitude and frequency. A complete development is given in the Appendix. Here we outline a simplified treatment that neglects microwave observer amplitude, h_1, saturation (such effects can be nearly corrected using the formula for R_{2e} in Eq. [2]).

The resonance expression for the Lorentzian line including the first harmonic of the modulation frequency (ω_m) is, in complex form,

$$a_1^{\pm} = a_0 \pm \omega_m, \quad [3]$$

where $a_0 = \Delta + i \cdot R_{2e}$ defines the (complex) Lorenztian lineshape (a_0^{-1}) in the absence of modulation. $\Delta = \omega - \omega_0$ is the frequency offset from the resonance frequency ω_0, and $R_{2e} = 1/\gamma \cdot T_{2e}$ is the linewidth. The effects of Zeeman modulation amplitude h_m are incorporated in three terms, $g_1^{\pm}$ and g_0:

$$g_1^{\pm} = \frac{1}{2} a_1^{\pm}\{1 + \sqrt{1 - (\gamma h_m/a_1^{\pm})^2}\} \quad [4a]$$

and

$$g_0 = a_0 - (\gamma h_m/4)\{1/g_1^+ + 1/g_1^-\}. \quad [4b]$$

The EPR signals are complex numbers of which the dispersion is the real part and the absorption is the imaginary part: Sig_1 is the in-phase, first harmonic signal, and Sig_1^Q is the phase-quadrature, first-harmonic signal. The complex EPR signals are linear combinations of the products of the g's:

$$Sig_1 = \frac{-1}{2\pi}\left\{\frac{1}{(g_0 g_1^+)} + \frac{1}{(g_0 g_1^-)}\right\} \quad [5a]$$

and

$$Sig_1^Q = \frac{-i}{2\pi}\left\{\frac{1}{(g_0 g_1^+)} - \frac{1}{(g_0 g_1^-)}\right\}. \quad [5b]$$

These are normalized relative to the area of the double integral of the in-phase absorption signal. Notice that when the modulation frequency and amplitude are set to zero, the pure (unmodulated) absorption and dispersion-shaped Lorentzian signals are recovered viz. $Sig_1 = -1/\pi a_0$. These equations execute very quickly and require minimally more time than the simulations without modulation effects.

INTRINSIC BROADENING MECHANISMS

Rotational correlation time. In simulating nitroxide spectra, we assume that each line due to the nitrogen nuclear hyperfine splitting (hfs) has its own, intrinsic, independent linewidth, and that the distance between the lines is arbitrary, even though the line positions are largely determined by the hfs. Other nuclei in the nitroxide molecule with non-zero super-hfs, e.g., neighboring protons or deuterons and naturally abundant ^{13}C nuclei, can split the spectrum further. These splittings may or may not be resolved depending on the line's width relative to the hfs; if not resolved they make the apparent linewidth broader. This effect is usually called inhomogeneous broadening for historical reasons—such apparent broadening of lines can also occur if there is an inhomogeneous Zeeman field over the sample. We found that incorporation of inhomogeneous broadening effects was essential for obtaining high-

quality lineshape simulations. The total hfs splitting is produced by first forming a binomial (or trinomial) distribution of stick spectra appropriate for the number of protons (or deuterons) contributing (*8*). After combining this pattern with that of other natural abundance isotopes, such as ^{13}C, the final stick pattern has the linewidth convolved onto it. For computation we perform these operations on the unpaired electron e^- as a series of convolutions: $e^- \otimes a_N \otimes a_{HorD} \otimes a_{c^{13}}$ where a_N, etc., represent the appropriate magnitude and type of hfs. In the 1970s Freed and co-workers extracted linewidths from experimental spectra in liquids (*9*) by such a convolution of Lorentzians with the appropriate hfs stick spectrum. Windram and Plachy employed this method in studies of spin-labeled lipid bilayers (*10*) as did Hyde and Subczynski in their work on CTPO in water (*11*). Recently workers have used the approximation of adding Lorentzians to a Gaussian broadening function to model unresolved hyperfine patterns (*12*). Selected points in the wings of the lines were used to extract the true Lorentzian assuming the shape was a sum of a Lorentzian and a Gaussian (*13*). Other work was done by Lee (*14*) and by Halpern (*15*). More recently a direct convolution of Lorentzian and Gaussian functions using the fast Fourier transform (FFT) algorithm has been reported (*16*). In our analyses the use of a Gaussian was not a good enough approximation of the hfs pattern, mainly because our signals had a very large SNR. We returned to directly simulating the correct hfs stick spectrum and convolving it with Lorentzian lines of appropriate width.

Concentration effects from paramagnetic molecules. The intermolecular processes arising from collisions of the spin labels with each other or with a paramagnetic molecule such as oxygen (when present) broaden the lines. The chance collision of molecules is a stochastic process and produces an exchange of spin states, resulting in a broader Lorentzian line for any non-zero concentration of paramagnetic molecules. Because collision frequency increases with increasing concentration homogeneous Lorentzian linewidths of the spectra will always be greater than the fundamental, intrinsic value of R_{2e} (*17*). Such processes increase the homogeneous linewidth of all lines by the same amount.

METHOD OF DATA ANALYSIS AND SIMULATION

Optimization strategy. In optimization programs one minimizes the deviation of the experimental line from the theory. If Y_i is the data point at the ith position in the spectrum, and $\hat{Y}_i$ the simulation, then the quantity to be minimized is the variance σ^2:

$$\sigma^2 = \frac{1}{N}\sum_{i=1}^{N}(Y_i - \hat{Y}_i)^2 = \langle (Y_i - \hat{Y}_i)^2 \rangle. \qquad [6]$$

This is the standard least-squares method—a very nonlinear process. The need to include an arbitrary scale, s, and baseline offset, b, adds two extra parameters that must be included in the search. These add no information on the linewidths and hence are of no interest unless a display of fit versus data is needed at the end. A more suitable model for lineshape analysis defines the variance with the s and b corrections explicitly included:

$$\sigma^2 = \frac{1}{N}\sum_{i=1}^{N}(Y_i - s\cdot\hat{Y}_i - b)^2. \qquad [7]$$

The variance of the data is

$$\sigma_y^2 = \langle (Y_i - \langle Y_i \rangle)^2 \rangle \qquad [8]$$

and that of the model is

$$\sigma_{\hat{y}}^2 = \langle (\hat{Y}_i - \langle \hat{Y}_i \rangle)^2 \rangle. \qquad [9]$$

The standard error is proportional to the correlation coefficient and the variance of the data

$$\sigma^2 = (1 - R^2)\sigma_y^2, \qquad [10]$$

where R is the correlation coefficient, corrected for the mean (*18*):

$$R = \frac{\langle (Y - \langle Y \rangle)\cdot(\hat{Y} - \langle \hat{Y} \rangle)\rangle}{\sigma_y \sigma_{\hat{y}}}. \qquad [11]$$

R is bounded by the triangular inequality ($-1 \le R \le 1$) and is a dimensionless way to represent the variance between the experiment and the theory or model—independent of the scaling or baseline offset of the data. R is maximized (σ minimized) using a Marquardt–Levenberg search. The overlaid fit can be found by computing s and b: $s = R\sigma_y/\sigma_{\hat{y}}$ and $b = \langle Y \rangle - s\langle \hat{Y} \rangle$ with the optimum scaling and baseline found by the setting the derivatives of σ^2 with respect to s and b to be zero. The scale factor, s, is calculated at the end of the fitting process.

The double integral of the $\hat{Y}_i$ spectrum is unity so that $\sigma_y/\sigma_{\hat{y}}$ is the ratio of the data and fit. The inclusion of R in s shows that a poor fit will lead to large errors in s as would be expected. This scale factor avoids some of the problems associated with the usual methods of double integration. For example, if the EPR signal has some asymmetry due to a slight mixture of dispersion into the absorption signal then even a noiseless double integral will be in error. The scale factor is the ratio of the magnitudes of spectra of the same (arbitrary) shape—no phase rotation is needed. The scale factor only uses

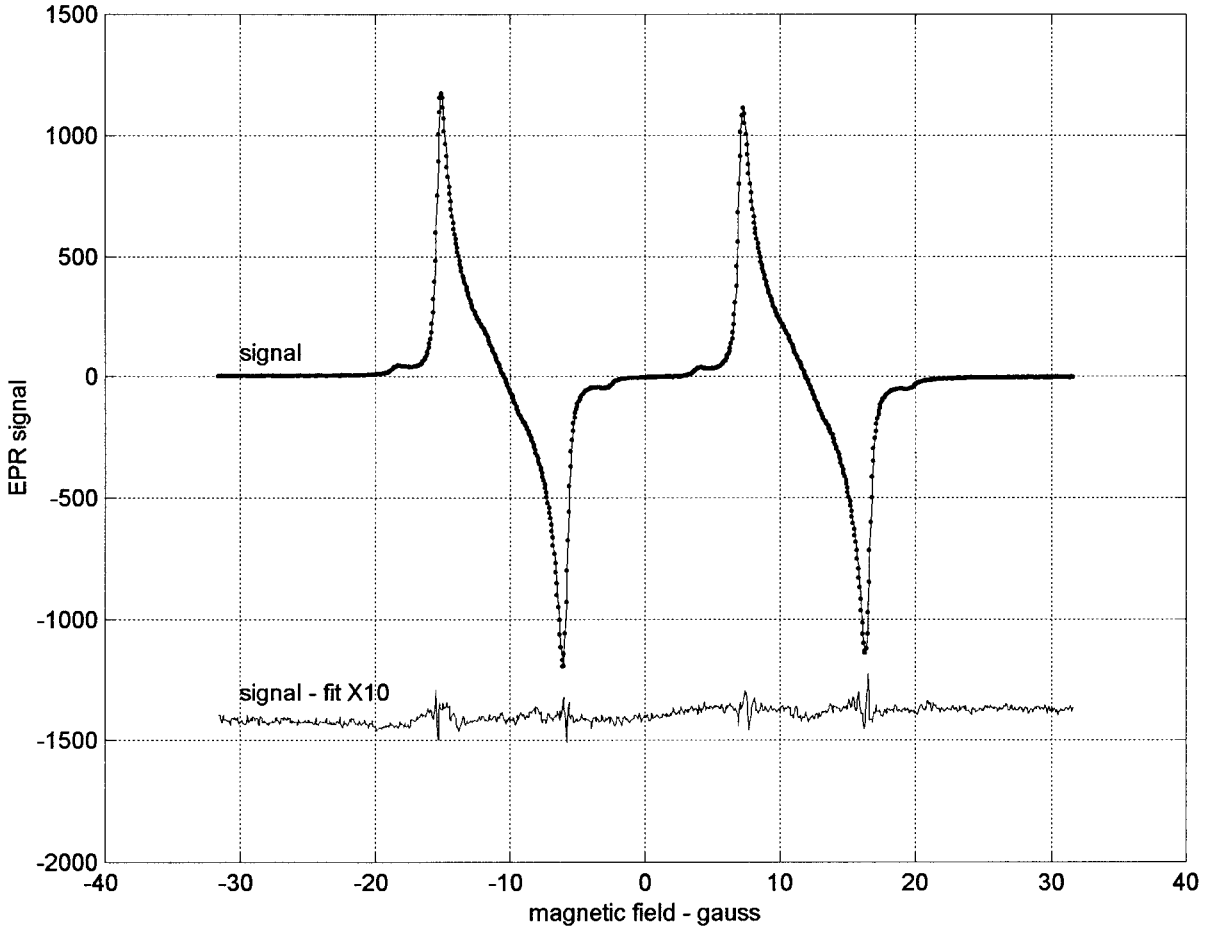

FIG. 1. The CW EPR spectrum of a sample that is a 2-mm-long 0.6 mM solution of $^{15}ND_{13}$ CTPO (2,2,5,5-tetramethyl-3-pyrrolin-d_{13}-1-^{15}N-1-oxyl-3-carboxamide) in water at room temperature, contained in a 0.8-mm OD × 0.6-mm ID capillary in a 1-mm loop gap resonator (Medical Advances, Milwaukee, WI). The least-squares best fit simulation is overlaid on the spectrum, and the residual (×10 gain) is shown below them. The spectrum was fit with the following parameters (in units of gauss): the two crossover points had optimized values of −10.588 and 11.791, the two linewidths were optimized at 0.240 and 0.264, the axial deuteron hfs splitting was 0.075 and the 12 equivalent deuterons had 0.031 hfs couplings, and the ring ^{13}C splittings were 6.07 and 6.90. In addition, the microwave observer amplitude h_1 was 0.04 G and the optimum microwave phase of the signal was 2°, i.e., virtually no dispersion component. The 10-kHz Zeeman modulation amplitude of 9.38 G produced a slight admixture of quadrature component so that the optimum Zeeman phase was 3°. The goodness of fit is determined from the closeness of the R value of Eq. [11] to unity: here $1 - R^2 = 1 \cdot 10^{-4}$. The χ^2 was 14.2 for this spectrum with a SNR of 372. All quantities measured in gauss have a standard error of ±0.005 G.

data from the spectral region where the signal is located unlike double integration which requires extended flat zero-baseline regions. For a well fit spectrum (R close to unity) the scale factor is controlled by $\sigma_{\hat{y}}$; this puts strong requirements on the model used for fitting the data. We have found that the s is sensitive to subtle details of the model used. Every effort must be made to reduce $\chi^2 = \sigma^2/\sigma_n^2$ to as low a value as possible for best $\sigma_{\hat{y}}$ and s.

Data analysis. Once a spectrum is acquired by the spectrometer and stored on disc the files are translated into the form needed for fitting to the spectral model chosen. On the screen are displayed all the parameters of the spectrum along with the options to float or fix any of the parameters. The procedure is to first optimize the derivative spectral crossover positions, the Lorentzian linewidths, microwave phase (absorption/dispersion components), and the ^{13}C hfs. The resulting microwave phase and ^{13}C hfs values are fixed and the crossover positions, Lorentzian linewidths, and deuteron (or proton) hyperfine splittings are allowed to vary. The entire fit is then redone allowing as many quantities to float as possible to ensure that the minimum χ^2 has been attained. It is essential that the crossovers and initial linewidths be optimized first; if this not done then the other parameters do not converge on stable meaningful values. The fitted spectrum, the scale factor, χ^2, and the signal-to-noise ratio are computed. The SNR is computed as the ratio of variance of the data, σ_y, to the variance of the noise, σ_n. We calculate σ_n by subdividing the 1024-point experimental spectrum into 8–10 segments and calculating the variance of each segment about a straight line—σ_n^2 is the smallest of

TABLE 1[a]

Peak-to-peak modulation amplitude (gauss)	Mean low-field linewidth (gauss)	Standard error (gauss)	Mean high-field linewidth (gauss)	Standard error (gauss)
1.00	0.134	0.005	0.160	0.006
0.50	0.131	0.005	0.157	0.006
0.25	0.142	0.006	0.167	0.005
0.10	0.149	0.002	0.173	0.002
0.025	0.144	0.007	0.169	0.009

[a] Sample was deoxygenated 0.1 mM $^{15}ND_{13}$ dCTPO in water for minimum linewidth using 10-kHz modulation frequency. Standard errors are those reported for these quantities due to the fit of the model to each of the data sets and do not necessarily reflect the overall accuracy of the values.

these variances. The value of SNR obtained in this way is an objective estimate of the SNR. A more common calculation of SNR is the ratio of the height of the largest peak-to-peak signal to the rms noise; our method removes the bias for narrow line spectra and makes use of all the information in the spectrum. Explicitly including the instrumental parameters is the fitting process allows for much more flexibility in data collection and makes for more accurate analysis, e.g., all data need not be collected at the same Zeeman modulation amplitude. Sample concentrations were calibrated using the scale factors of the fits to spectra of known concentration. The analysis also corrects for different instrumental parameters—amplifier gains, modulation amplitude, sample size, type of resonator, microwave power, number of scans, and acquisition time. Oxygen concentrations in the sample were calculated from the IUPAC solubility tables for oxygen–water and oxygen–glycerol mixtures (*19*). The microwave power and the spin–lattice relaxation rate were not optimized by the fitting procedure. Rather, the microwave power is a known fixed quantity, the spin–lattice relaxation rate has been measured independently (*20*), and their effects on the linewidth are corrected by Eq. [2].

RESULTS AND DISCUSSION

Figure 1 presents the results of the analysis of the solution spectrum of $^{15}ND_{13}$ deuterated CTPO (2,2,5,5-tetramethyl-3-pyrrolin-d_{13},1-^{15}N-1-oxyl-3-carboxamide) with the least-squares best fit overlaid on the data, and with the 10× expanded residual (signal minus fit) below. The modulation frequency, the modulation amplitude, and the observer amplitude were previously calibrated and not allowed to vary. The overall fit was excellent, except for the turning points: close inspection of the fitting at these points indicates that the spectrum was swept slightly too fast to truly reflect the narrow Lorentzian character of the spectra in this region where the signal is changing most rapidly.

Zeeman modulation. A test of the Zeeman modulation correction is how well the program and procedure can model over modulation. The excellent fit in Fig. 1 clearly shows it is successful. For the 2-mm-long CTPO "point" sample used—the intrinsic Lorentzian, modulation corrected, $^{15}ND_{13}$ linewidths are 0.24 and 0.26 G, respectively. The agreement with experiment is excellent as given by the low χ^2 of 14.2—even though each line is broadened and distorted by the large modulation amplitude of 9.38 G peak-to-peak at 10 kHz. As further proof Table 1 shows the results of fitting spectra of a sample of deoxygenated 0.1 mM $^{15}ND_{13}$ CTPO in water over a range of modulation amplitudes: the simulations extracted similar intrinsic Lorentzian linewidths independent of modulation amplitude. The line can be overmodulated by up to 20 times the intrinsic width but the result is still the intrinsic linewidth with no penalty in fitting accuracy. We should add that if there is a distribution of modulation amplitudes over the active volume of the sample the fitting program cannot correct for overmodulation greater than about a factor of four times the intrinsic linewidth. The error that results is an increase in the fitted linewidth of about 10%. Parenthetically, we note that this program provides any easy way to calibrate the Zeeman modulation amplitude at any Zeeman frequency. We emphasize that it is the ratio of the modulation amplitude to the true Lorentzian linewidth that determines the degree of overmodulation, not the ratio of modulation amplitude to the apparent width of the spectral line.

Halpern *et al.* (*15*) have modeled the effects of inhomogeneous broadening on Lorentzian lines by using an appropriate sum of Lorentzian and Gaussian lines and extracting the Lorentzian widths. Subsequently their analysis was extended to overmodulated Voigtian lines (*21*). They showed that the amplitude at which the maximum EPR signal was observed varied as the ratio of Lorentzian to Gaussian widths, and this could be used to get the ratio. Knowing this ratio and the observed linewidth the actual values of the Lorentzian and Gaussian linewidths at zero-modulation amplitude could be obtained. As a result the corrected Lorentzian linewidth could be obtained from a spectrum slightly distorted by overmodulation (where the effect of the distortion was to simply increase the apparent width of the Gaussian component). If we removed the modulation correction from our program and floated the hfs split-

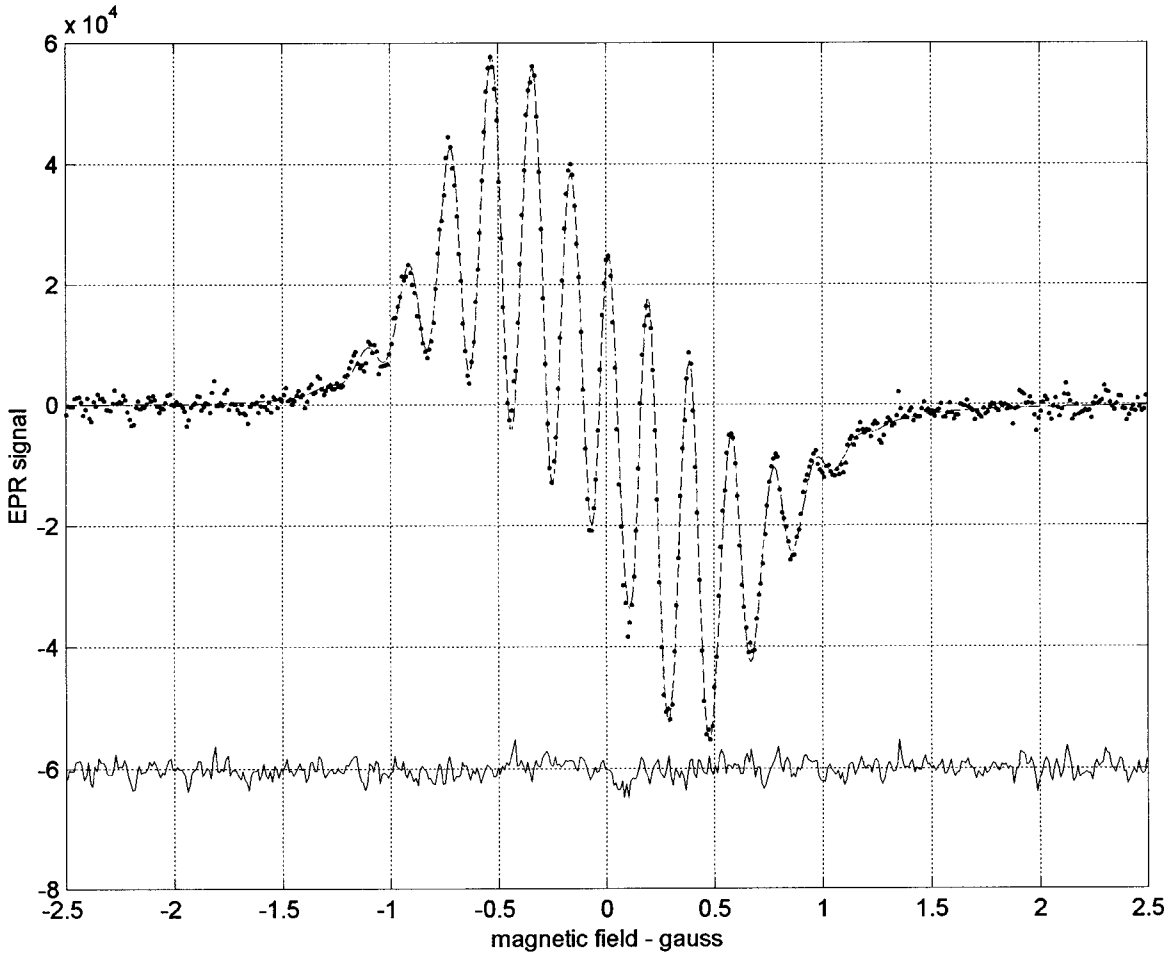

FIG. 2. The EPR spectrum of the center line of deoxygenated 0.1 mM of $^{14}NH_{13}$ CTPO in water (●) and the fit (dashed line) with the residual (signal-fit) below. The best ($\chi^2 = 2.9$) Lorentzian linewidth found by the program was 0.102 ± 0.005 G. The spin–lattice relaxation rate, R_{1e}, is equivalent to a linewidth of 0.057 G in this sample (*20*); a microwave field h_1 of amplitude 0.04 G (measured independently) was used to observe the signal. These conditions, from Eq. [2], result in saturation brodening of the line by 0.015 G; when this is subtracted the corrected estimate for the true homogeneous linewidth is 0.087 ± 0.005 G.

tings then the apparent hfs similarly increased to absorb overmodulation effects. These corrections for overmodulation by changes in hfs or Gaussian width are artificial and clearly nonphysical. At the large modulation amplitudes used to obtain the spectrum of Fig. 1 a simple Lorentzian–Gaussian sum would never fit the spectral shape; a full simulation must be done. Smirnov and Belford (*16*) used a direct convolution of Lorentzian and Gaussian functions by FFT to extract the true Lorentzian width from a Voigtian line. Morse *et al.* (*22*) have elegantly applied this technique to study the kinetics of oxygen uptake in cells, and Smirnov *et al.* (*23*) measured oxygen permeability in phospholipid bilayers. Their method required that the experimental conditions be unchanged; our ability to correct for both Zeeman modulation amplitude and power saturation broadening lifts this restriction. Figure 2 shows the spectrum, fit, and residual for the central region of $^{14}NH_{13}$ protonated CTPO with oxygen removed. The χ^2 of 2.9 confirms that the model of 12 methyl protons with hyperfine splitting of 0.193 G split by one axial proton with a hyperfine splitting of 0.518 G is a very good one. These results are in excellent agreement with the those of Hyde and Subczynski (*11*) for the same molecule at the same nominal concentration—their fits gave a linewidth of 90 mG with axial and methyl proton coupling constants of 0.19 and 0.52 G at 20°C (data calculated from Fig. 3 of Ref. (*11*)).

Exchange effects. Figure 3 (bottom) shows the experimental EPR signal with fit overlaid and residual from dCTPO that has approximately a 1-G linewidth obtained at 8 mM label concentration. We used the same protocol that produced the results in Figs. 1 and 2—we allowed linewidths and crossovers to vary for best χ^2 and then did the same to all the hyperfine splittings, as described above. The apparent hyperfine coupling decreased for this more concentrated sample. We expected to get a similar high quality of fit, with low χ^2. In fact the best fit contains a large residual suggesting that the intrinsic lineshape

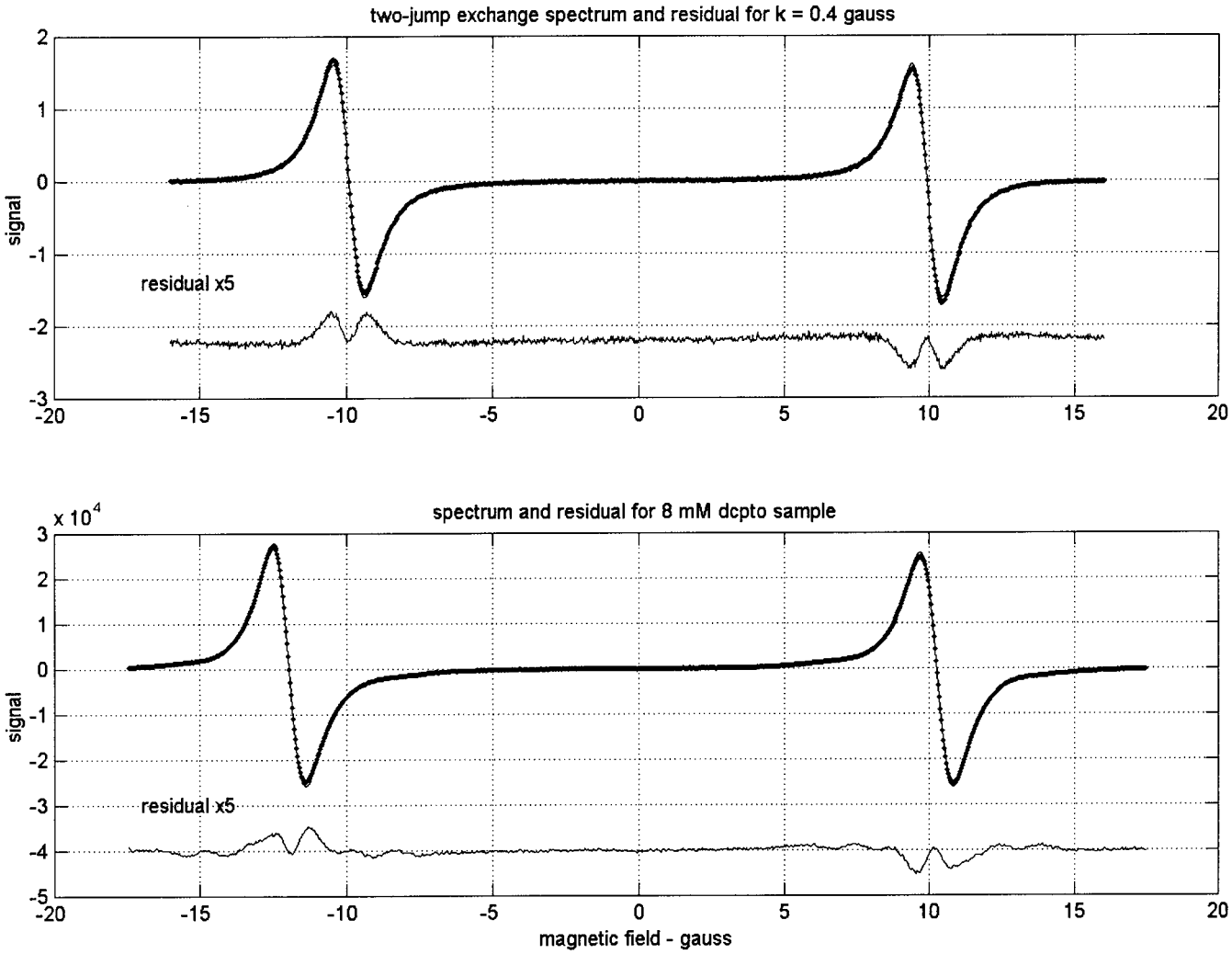

FIG. 3. (Top) Simulated two-jump slow exchange spectrum with an exchange rate constant of 400 mG and a hyperfine splitting of 20 G; the intrinsic (no exchange) linewidth is 100 mG. Random noise has been added for a SNR of 100. The residual is the difference between the simulated spectrum and the fit is shown with 5× gain. (Bottom) Spectrum of spin-labeled $^{15}ND_{13}$ CTPO in water. Linewidths are approximately 800 mG and the nitrogen hyperfine splitting is 22.2 G. The linewidths as well as the deuteron hyperfine coupling were allowed to freely float to find optimum values. The optimum deuteron value was less in this spectrum than in the lower concentration spectra (see Ref. (*26*)). The residual is the 5× difference between the experimental spectrum and the result of fitting it with the fitting program. This large residual shape appears in both spectra and demonstration of this fact is the main point of this figure (see text).

is no longer pure Lorenztian. This is unexpected as we are in the conditions for very slow exchange (*17*)—line broadening is very much less than the spectral line separation—and would expect the lineshapes still to be pure Lorentzian. Figure 3 (top) is the result of simulating the exchange process with a two-site jump model (*17, 24*). Fitting this theoretical spectrum with our analysis protocol produced a residual of the same form as for the experimental spectrum. This is a clear indication that the exchange process causes this line distortion—not an artifact of the analysis. The residual is symmetric about the line center and therefore cannot be due to an extra absorption derivative component. The fact that the residual has opposite signs for the two lines means that it cannot be due to a dispersion component, which would have the same sign for both. Molin's (*17*) theory also predicts that the inward shift of the line positions is quadratic in spin label concentration. In our experience, and that of Halpern (*25*), this shift appears linear in concentration. The implications of these results will be discussed in the accompanying experimental paper (Paper II) (*26*).

CONCLUSIONS

We have developed a useful, general method for measurement of linewidths—even in the face of overlapping spectra—using a widely available commercial software package. As a practical matter the ability to correct for Zeeman overmodula-

tion allows higher amplitudes to be used with corresponding higher signal-to-noise ratio. A surprising finding was that saturation broadening effects on the EPR lines were nonnegligible; the linewidths must be corrected. At high spin label concentrations the effects on the lineshape of intermediate spin exchange can be observed. An improved method has been developed for estimating relative spin concentrations by obtaining the scale factor between the data and a best fit spectrum of unit area. An important feature of this method is that the quality of the fit can give estimates of the errors in the scale factor.

APPENDIX—ZEEMAN MODULATION CORRECTION

To a large extent other workers have avoided simulation of Zeeman modulation effects apart from early studies in the 1960s (*5*). Recently Hyde (*27*) introduced the mathematical technique of pseudo-modulation with the primary aim of transforming absorption-shaped EPR spectra into absorption derivative spectra without a decrease in signal-to-noise ratio. These authors kindly supplied us with a computer program (SUMSPEC 2) and we found that it could simulate the lineshapes of overmodulated lines. The theory for the nonlinear EPR technique of ST EPR developed by us in the 1970s includes the effects of modulation explicitly (*7*).

We consider a single spin-$\frac{1}{2}$ particle in the presence of a DC magnetic field, a microwave RF source, and a Zeeman modulation source. The Hamiltonian (in frequency units) including these three interactions in the rotating frame is

$$H = \Delta S_z + \gamma h(S_+ + S_-) + \gamma h_m S_z \cos(\omega_m t),$$

where $\Delta = \omega_o - \omega$ is the frequency difference between the Larmor precession frequency of the spin, ω_o, and the frequency of the applied radiofrequency (RF), ω. $h = h_1$ of the text, and is the amplitude of the RF in Gauss. The associated density matrix equation of motion is

$$\dot{\chi} = -i[H, \chi] - i\beta[(S_+ + S_-), S_z] - \Gamma(\chi), \quad \text{[A-1]}$$

where $\beta = \gamma h\, \hbar\omega_o/k_B T$. The presence of the h_m Zeeman term causes modulation of the components of the magnetization. For a spin-1/2 particle the equation of motion requires the 2 by 2 representation of the spin operators (*28*):

$$H = \begin{pmatrix} \Delta/2 + \gamma h_m/2 \cos(\omega_m t) & \gamma h \\ \times & -(\Delta/2 + \gamma h_m/2 \cos(\omega_m t)) \end{pmatrix}, \quad \text{[A-2]}$$

and the relaxation matrix is

$$\Gamma(\chi) = \begin{pmatrix} \tfrac{1}{2}R_1(\chi_{11} - \chi_{22}) & R_2\chi_{12} \\ R_2\chi_{21} & -\tfrac{1}{2}R_1(\chi_{11} - \chi_{22}) \end{pmatrix}. \quad \text{[A-3]}$$

The longitudinal signal is $L = \langle S_z \rangle = \mathrm{tr}\{S_z\chi\} = \frac{1}{2}(\chi_{22} - \chi_{11})$.

The equations of motion then are

$$\frac{d}{dt}\begin{pmatrix} \chi_{11} & \chi_{12} \\ \chi_{21} & \chi_{22} \end{pmatrix} = -i\begin{pmatrix} \gamma h(\chi_{12} - \chi_{21}) & \\ -\{\Delta + \gamma h_m \cos(\omega_m t)\}\chi_{21} - 2\gamma h L & \times \end{pmatrix} \begin{matrix} \\ \{\Delta + \gamma h_m \cos(\omega_m t)\}\chi_{12} + 2\gamma h L \\ -\gamma h(\chi_{12} - \chi_{21}) \end{matrix} \Bigg) - \begin{pmatrix} -R_1 L & R_2\chi_{12} \\ R_2\chi_{21} & R_1 L \end{pmatrix} - i\beta\begin{pmatrix} 0 & 1 \\ -1 & 0 \end{pmatrix}. \quad \text{[A-4]}$$

The observed signals are the absorption (A) and dispersion (D) components of the magnetization:

$$\begin{pmatrix} D \\ A \end{pmatrix} = \begin{pmatrix} \mathrm{tr}\{S_x\} \\ \mathrm{tr}\{S_y\} \end{pmatrix} = \begin{pmatrix} \frac{1}{2}(\chi_{12} + \chi_{21}) \\ \frac{1}{2i}(\chi_{12} - \chi_{21}) \end{pmatrix}. \quad \text{[A-5]}$$

After rearranging for the different elements,

$$\begin{aligned} \dot{L} &= -2\gamma h(A) - R_1 L \\ \dot{D} &= -\{\Delta + \gamma h_m \cos(\omega_m t)\}A - R_2 D \\ \dot{A} &= \{\Delta + \gamma h_m \cos(\omega_m t)\}D - R_2 A + 2\gamma h L + \beta. \end{aligned} \quad \text{[A-6]}$$

The equations of motion for the three signals are explicitly time dependent only in terms of the Zeeman modulation frequency. Therefore, it is simplest to do a Fourier expansion in terms of the harmonics of the modulation:

$$\begin{pmatrix} D(t) \\ A(t) \\ L(t) \end{pmatrix} = \sum_{r=-\infty}^{\infty} \exp(ir\omega_m t)\begin{pmatrix} D_r \\ A_r \\ L_r \end{pmatrix}. \quad \text{[A-7]}$$

Substitution into the above equations shows that

$$\begin{pmatrix} -r\omega_m & R_1 \\ R_1 & r\omega_m \end{pmatrix}\begin{pmatrix} L_r \\ L'_r \end{pmatrix} = -2\gamma h\begin{pmatrix} A'_r \\ A_r \end{pmatrix}, \quad \text{[A-8]}$$

which can be rearranged to solve for L_r in terms of A_r:

$$\begin{pmatrix} L_r \\ L'_r \end{pmatrix} = \frac{-2\gamma h}{r\omega_m^2 + R_1^2}\begin{pmatrix} R_1 & -r\omega_m \\ r\omega_m & R_1 \end{pmatrix}\begin{pmatrix} A_r \\ A'_r \end{pmatrix}. \quad \text{[A-9]}$$

The transverse components may be expanded in a Fourier

series, and one finds that the equations for the dispersion components are

$$\begin{pmatrix} 0 & r\omega_m \\ -r\omega_m & 0 \end{pmatrix}\begin{pmatrix} D_r \\ D'_r \end{pmatrix} = \begin{pmatrix} -\Delta & 0 \\ 0 & -\Delta \end{pmatrix}\begin{pmatrix} A_r \\ A'_r \end{pmatrix} + \begin{pmatrix} -\frac{1}{4}\gamma h_m & 0 \\ 0 & -\frac{1}{4}\gamma h_m \end{pmatrix} \times \left\{ \begin{pmatrix} A_{r-1} \\ A'_{r-1} \end{pmatrix} + \begin{pmatrix} A_{r+1} \\ A'_{r+1} \end{pmatrix} \right\} + \begin{pmatrix} -R_2 & 0 \\ 0 & -R_2 \end{pmatrix}\begin{pmatrix} D_r \\ D'_r \end{pmatrix}. \quad [A\text{-}10]$$

The absorption components may be similarly expanded and the longitudinal components substituted into the equation for the absorption components. After a little rearrangement the set of 4 by 4 equations for each harmonic may be generated. The in-phase and phase quadrature components of the absorption can then be substituted back into the equations for the four absorption and dispersion signals:

$$\underline{A}_r \mathbf{X}_r + \left(\frac{\gamma h_m}{4}\right)\{\mathbf{X}_{r+1} + \mathbf{X}_{r-1}\} = \delta_{r,o}\mathbf{Z}, \quad [A\text{-}11]$$

where the vector of elements X is

$$\mathbf{X}_r = \begin{pmatrix} A_r \\ D_r \\ D'_r \\ -A'_r \end{pmatrix}.$$

The choice of $-A'_r$ in the signal vector is a phase convention to make the matrices more symmetric. The matrix A_r is a 4 by 4 matrix with the resonance condition on the diagonal.

$$\underline{A}_r = \begin{pmatrix} \Delta & -R_2 & r\omega_m & 0 \\ R_2 + R_1 S_r & \Delta & 0 & r\omega_m(1 - S_r) \\ r\omega_m(1 - S_r) & 0 & \Delta & -(R_2 + R_1 S_r) \\ 0 & r\omega_m & R_2 & \Delta \end{pmatrix}, \quad [A\text{-}12]$$

where S_r is the dimensionless, saturation parameter from the longitudinal term

$$S_r = \frac{(\gamma h)^2}{(r\omega_m)^2 + (R_1)^2} \quad [A\text{-}13]$$

and Z is the column, inhomogeneous vector

$$\bar{Z} = \beta \cdot \begin{pmatrix} 0 \\ 1 \\ 0 \\ 0 \end{pmatrix}.$$

The in-phase components are even under exchange of r for $-r$, therefore,

$$\mathbf{X}_1 + \mathbf{X}_{-1} = 2\underline{M}\mathbf{X}_1 \text{ where } \underline{M} = \begin{pmatrix} 1 & 0 & 0 & 0 \\ 0 & 1 & 0 & 0 \\ 0 & 0 & 0 & 0 \\ 0 & 0 & 0 & 0 \end{pmatrix}, \quad [A\text{-}14]$$

which is needed for the $r = 0$ equation.

The Recursive Solution

To solve for the r components we consider this to be a recursive problem viz. if $X_{(r+1)}$ is known we can solve for X_r. This is equivalent to a tridiagonal matrix problem, which has the form from the coupled equations as (*7, 28*)

$$\begin{pmatrix} \underline{A_0} & \frac{\gamma h_m}{2} M & 0 & 0 & 0 \\ \frac{\gamma h_m}{4} & \underline{A_1} & \frac{\gamma h_m}{4} & 0 & 0 \\ 0 & \frac{\gamma h_m}{4} & \underline{A_2} & \frac{\gamma h_m}{4} & 0 \\ 0 & 0 & \frac{\gamma h_m}{4} & \underline{A_3} & \frac{\gamma h_m}{4} \\ 0 & 0 & 0 & \frac{\gamma h_m}{4} & \underline{G_n} \end{pmatrix}\begin{pmatrix} X_0 \\ X_1 \\ X_2 \\ X_3 \\ X_n \end{pmatrix} = \begin{pmatrix} \mathbf{Z}_0 \\ 0 \\ 0 \\ 0 \\ 0 \end{pmatrix}. \quad [A\text{-}15]$$

The recurrence begins with defining a new matrix G, in the lower right-hand corner at the maximum r value of n: $G_n = A_n$ then continue recursively which removes the upper triangular part of the matrix

$$G_r = A_r - \left(\frac{\gamma h_m}{4}\right)^2 (G_{r+1})^{-1},$$

and the signal at $r = 0$ is

$$G_0 = A_0 - 2\left(\frac{\gamma h_m}{4}\right)^2 M(G_1)^{-1}.$$

Once these definitions have been developed, $\mathbf{X}_0 = G_0^{-1}\mathbf{Z}_0$. Notice that as the modulation goes to zero, then $G_r = A_r$, as expected.

In an upward recursive manner, each of the signals can be found from

$$\mathbf{X}_r = -\frac{\gamma h_m}{4} G_r^{-1}\mathbf{X}_{r-1}. \quad [A\text{-}16]$$

Therefore the signal at the first harmonic X_1 is

$$\mathbf{X}_1 = -\tfrac{1}{4}\gamma h_m G_1^{-1} G_0^{-1}\mathbf{Z}_0 = -\tfrac{1}{4}\gamma h_m (G_0 G_1)^{-1}\mathbf{Z}_0$$
$$= -\tfrac{1}{4}\gamma h_m (A_0 G_1 - 2(\tfrac{1}{4}\gamma h_m)^2 M)^{-1}\mathbf{Z}_0. \qquad \text{[A-17]}$$

This type of recurrence often requires starting at $n \sim 30$ or so. However, examination of the recurrence formula shows that convergence can be hastened because the A_r matrices are very weakly dependent on r and are almost all alike. In particular if we suggest that $A_r = A_n$ for all $r > n$, then G_n can be found directly, because the only stationary point in the convergence of such a series is when $G_n = G_{n+1}$. Let us call this $G_n = C_n$, for converged G_n. The recurrence formula then is a self-consistent equation for C_n:

$$C_n = A_n - \left(\frac{\gamma h_m}{4}\right)^2 (C_n)^{-1},$$

and C_n must satisfy the quadratic equation

$$(C_n)^2 - A_n C_n + \left(\frac{\gamma h_m}{4}\right)^2 = 0.$$

The solution to this quadratic is

$$C_n = \tfrac{1}{2}A_n\{1 + \sqrt{1 - (\tfrac{1}{2}\gamma h_m)^2 (A_n)^{-2}}\}. \qquad \text{[A-18]}$$

This result is a formal one because the square root of a matrix is only defined in terms of the eigenvalues of the matrix. The solution chosen from the two possible is the one which has $C_n = A_n$ in the limit of zero-modulation amplitude. From the above equation it follows that A and C must commute. Therefore we can diagonalize the A matrix, which also diagonalizes the C matrix, and each element can be solved for independently. The final C matrix can be found by transforming the diagonalized C matrix back into its original form. The remarkable finding upon using this accelerated recurrence method is that it works extremely well for $n = 1$—the answer is nearly analytical; $G_1 = C_1$ is all that is needed to fit with experiment. The signal at the first harmonic may be written in its complex form by making the signal be Sig $= D + iA$ and Sig$' = D' + iA'$. Then

$$\begin{pmatrix} \text{Sig} \\ \text{Sig}' \end{pmatrix} = \frac{-1}{\pi}\begin{pmatrix} -i & 1 & 0 & 0 \\ 0 & 0 & -1 & -i \end{pmatrix}\mathbf{X}_1. \qquad \text{[A-19]}$$

This gives the in-phase and phase quadrature signals as complex quantities.

Nonsaturation case. When saturation is small, $S_r \sim 0$ and $h \sim 0$, and can be neglected; the A_r matrix simplifies and can be diagonalized by a transformation that does not depend on the modulation index, r. The transformation matrix, T, is

$$T = \frac{1}{2}\begin{pmatrix} -i & 1 & i & -1 \\ -i & 1 & -i & 1 \\ -i & -1 & i & 1 \\ -i & -1 & -i & -1 \end{pmatrix}.$$

The resulting diagonal matrix is

$$\underline{TA_rT^{-1}} = \begin{pmatrix} \Delta + iR_2 - r\omega_m & 0 & 0 & 0 \\ 0 & \Delta + iR_2 + r\omega_m & 0 & 0 \\ 0 & 0 & \Delta - iR_2 - r\omega_m & 0 \\ 0 & 0 & 0 & \Delta - iR_2 + r\omega_m \end{pmatrix}, \qquad \text{[A-20]}$$

where

$$TZ_r = \delta_{r,o}\beta\tfrac{1}{2}\begin{pmatrix} 1 \\ 1 \\ -1 \\ -1 \end{pmatrix}$$

and

$$TMT^{-1} = \frac{1}{2}\begin{pmatrix} 1 & 1 & 0 & 0 \\ 1 & 1 & 0 & 0 \\ 0 & 0 & 1 & 1 \\ 0 & 0 & 1 & 1 \end{pmatrix}.$$

This is in a blocked form so that the equations for the first two elements of Y are independent of the equations for the second two elements.

Therefore the equations for

$$\mathbf{Y}_r = T\mathbf{X}_r = \begin{pmatrix} Y_1^r \\ Y_2^r \\ Y_3^r \\ Y_4^r \end{pmatrix} = \begin{pmatrix} Y_+^r \\ Y_-^r \\ -Y_+^{r*} \\ -Y_-^{r*} \end{pmatrix}$$

separate into individual equations. There are only two equations because there are only two eigenvalues $a_r^{\pm} = \Delta + iR_2 \pm r\omega_m$; symmetry determines that $Y_3 = -Y_1^*$ and $Y_4 = -Y_2^*$. Therefore we only need to solve for the first two. The downward recurrence formula is $g_r^{\pm} = a_r^{\pm} - (\gamma h_m/4)^2 (g_{r+1}^{\pm})^{-1}$ and is initiated in the same way as above: viz. the stationary recurrence leads to a quadratic equation of g at some maximum r value, n:

$$g_n^{\pm} = \tfrac{1}{2}a_n^{\pm}\left\{1 + \sqrt{1 - \left(\frac{\gamma h_m}{2a_n^{\pm}}\right)^2}\right\}, \qquad \text{[A-21]}$$

and then downward recurrence is used. When $r = 0$ $a_0 = a_0^+ = a_0^-$, and we can regroup the equation

$$g_0 = a_0 - \left(\frac{\gamma h_m}{4}\right)\left\{\frac{1}{g_1^+} + \frac{1}{g_1^-}\right\}. \qquad \text{[A-22]}$$

With all the g's defined, the signals can be computed beginning with the $r = 0$ signal $Y_0^{\pm} = g_0^{-1}\tfrac{1}{2}\beta$ and recurring upward with $Y_r^{\pm} = -\gamma h_m/4\ g_r^{\pm -1} Y_r^{\pm}$. The complex signals are formed by recombining the Y's:

$$\begin{pmatrix} \mathrm{Sig}_r \\ \mathrm{Sig}_r' \end{pmatrix} = \frac{-1}{\pi}\begin{pmatrix} 1 & 1 \\ i & -i \end{pmatrix}\begin{pmatrix} Y_r^+ \\ Y_r^- \end{pmatrix},$$

and the first ($r = 1$) harmonic signals are

$$\begin{pmatrix} \mathrm{Sig}_1 \\ \mathrm{Sig}_1' \end{pmatrix} = -\frac{\beta}{2\pi}\cdot\frac{\gamma h_m}{4}\, g_0^{-1}\begin{pmatrix} 1 & 1 \\ i & -i \end{pmatrix}\begin{pmatrix} g_1^{+\,-1} \\ g_1^{-\,-1} \end{pmatrix}. \qquad \text{[A-23]}$$

The signals are scaled so that the absorption signal integrates to unit area: this is done by setting $\beta = 1$ in Eq. [A-23]. As with the full matrix approach the self-consistent downward recurrence can begin at $n = 1$ with remarkable accuracy and generates nearly analytical forms for the signals.

ACKNOWLEDGMENTS

We thank NIH for support for this work on P01-GM32681 and for a training grant for A. W. Reese. The EMX EPR spectrometer used was funded under the UW Environmental Sciences Center Grant P30-ESO7033 from NIEHS.

REFERENCES

1. G. Likhtenshtein, "Spin Labeling Methods in Molecular Biology," Wiley, New York (1974).
2. B. H. Robinson, A. W. Reese, and C. Mailer, 37th Rocky Mountain Conference on Analytical Chemistry, Denver, CO (1995).
3. W. Froncisz and J. S. Hyde, *J. Magn. Reson.* **47,** 515–521 (1982).
4. C. Mailer, D. A. Haas, E. J. Hustedt, J. G. Gladden, and B. H. Robinson, *J. Magn. Reson.* **91,** 475–496 (1991).
5. J. C. P. Poole, "Electron Spin Resonance: A Comprehensive Treatise on Experimental Technique," Wiley, New York (1983).
6. L. R. Dalton, B. H. Robinson, L. A. Dalton, and P. Coffey, *in* "Advances in Magnetic Resonance" (J. S. Waugh, Ed.), Vol. 8, p. 149, Academic Press, New York (1976).
7. B. H. Robinson, *J. Chem. Phys.* **78,** 2268–2273 (1983).
8. J. A. Weil, J. R. Bolton, and J. E. Wertz, "Electron Paramagnetic Resonance Elementary Theory and Practical Applications," Wiley, New York (1994).
9. J. S. Hwang, R. P. Mason, L. P. Hwang, and J. H. Freed, *J. Phys. Chem.* **79,** 489–511 (1975).
10. D. A. Windram and W. Z. Plachy, *Biochim. Biophys. Acta* **600,** 655–665 (1980).
11. J. S. Hyde and W. K. Subczynski, *J. Magn. Reson.* **56,** 125–130 (1984).
12. B. L. Bales, *in* "Spin Labeling: Theory and Applications" (L. J. Berliner and J. Reuben, Eds.), Vol. 8, p. 1–130, Plenum, New York (1989).
13. B. L. Bales, *J. Magn. Reson.* **38,** 193–205 (1980).
14. S. Lee and A. Shetty, *J. Chem. Phys.* **83,** 499–505 (1985).
15. H. J. Halpern, M. Peric, C. Yu, and B. L. Bales, *J. Magn. Reson. A* **103,** 13–22 (1993).
16. A. I. Smirnov and R. L. Belford, *J. Magn. Reson. A* **113,** 65–73 (1995).
17. Y. N. Molin, K. M. Salikhov, and K. I. Zamaraev, "Spin Exchange: Principles and Applications in Chemistry and Biology," Springer-Verlag, Berlin (1980).
18. A. L. Edwards, "Statistical Analysis," Holt, Rinehart & Winston, New York (1969).
19. R. Battino, H. L. Clever, and C. L. Young, "The Solubility of Gases in Liquids," Pergamon, Elmsford, NY (1981).
20. B. H. Robinson, D. A. Haas, and C. Mailer, *Science* **263,** 490–3 (1994).
21. M. Peric and H. J. Halpern, *J. Magn. Reson. A* **109,** 198–202 (1994).
22. P. D. I. Morse and A. I. Smirnov, *Magn. Reson. Chem.* **33,** S46–52 (1995).
23. A. I. Smirnov, R. B. Clarkson, and R. L. Belford, *J. Magn. Reson. B* **111,** 149–157 (1996).
24. A. Carrington and A. D. McLachlan, "Introduction to Magnetic Resonance with Applications to Chemistry and Chemical Physics," Chapman & Hall, London (1979).
25. H. J. Halpern, M. Perc, T.-D. Nguyen, B. A. Teicher, Y. J. Lin, and M. K. Bowman, *J. Magn. Reson.* **90,** 40–51 (1990).
26. B. H. Robinson, C. Mailer, and A. W. Reese, *J. Magn. Reson.* **138,** 210–219 (1999).
27. J. S. Hyde, M. Pasenkiewicz-Gierula, A. Jesmanowicz, and W. E. Antholine, *Appl. Magn. Reson.* **1,** 483–496 (1990).
28. B. H. Robinson and L. R. Dalton, *Chem. Phys.* **36,** 207–237 (1979).